Journal of Materials and Engineering Structures

Research Paper

Stability of Cracked Plates with Nonlinearly Variable Thickness Resting on Elastic Foundations

Le Vinh An, Pham Minh Phuc, Bui Tuan Anh*

University of Transport and Communications, 3 Cau Giay Street, Dong Da District, Hanoi city, Vietnam

ARTICLE INFO

Article history:

Received : 15 November 2022

Revised : 25 December 2022

Accepted : 28 December 2022

Keywords:

Cracked plates

Nonlinearly Variable Thickness

Elastic foundations

Stability

ABSTRACT

In this paper, the stability of rectangular cracked plates with nonlinearly variable thickness resting on the elastic foundations is studied. The thickness of the plate varies exponentially along the x-axis. Meanwhile, the elastic foundation is modeled by a two-parameter Pasternak elastic foundation type. The crack is assumed at the center of the plate with variable length and angle of inclination. The establishment of the stability equations of the cracked plate is based on the Higher Order Shear Deformation Theory (HSDT) combined with the phase field theory. Next, using the finite element method to solve the equations to find the minimum force that causes plate instability. To test the reliability of the computational theory, the results are compared with several reputable published papers. Then, the article will investigate the influence of elastic foundation, crack location, crack length and crack inclination on the stability of plate. The results show that the elastic foundation has a great influence on the plate stability, while the crack inclination angle has less influence. Finally, there are some images of the destabilization patterns of cracked plates placed on an elastic foundation.

F. ASMA & H. HAMMOUM (Eds.) special issue, 4th International Conference on Sustainability in Civil Engineering ICSCE 2022, Hanoi, Vietnam, J. Mater. Eng. Struct. 9(4) (2022)

1 Introduction

The failure of the structure is understood as the change in the physical properties (materials, connections, ...) and geometry (sizes, shapes, ...) compared to the intact texture. Structural damage is generally described by two parameters: location and extent of damage. Crack is a typical failure of a structure, characterized by two parameters, its position and size.

To calculate the stability of cracked plates, there are several methods such as finite element method (FEM), extended finite element method (XFEM), isogeometric analysis (IGA), phase field method and so on… In which, the phase field method has the advantage of simulating cracks through the variable phase field changing from 0 to 1. This makes the structure continuous, which helps to reduce the calculation process. Recently, the phase field method has been extensively developed to study the stability and vibration of the cracked plate which studied by Phuc et al. [1-6].

* *Corresponding author. Tel.: +84.904.127.393*
E-mail address: tuananh.bui@utc.edu.vn

e-ISSN: 2170-127X, (cc) BY-SA

RESEARCH REVIEW of Sciences and Technologies

Recently, the applications of plate structures with more complex physical shapes are used in the engineering field due to their high aesthetics. However, the disadvangtage of this structure type is the damage caused by instability that is more different from the flat plate structures, especially due to the influence of plate cracks. However, the disadvantage of this type of structure is that the damage due to instability is more different from the flat plate structure, especially due to the influence of cracks and the variable thickness, the instability of the plate structure will become more complicated. Wittrik & Ellen [7] studied the buckling stress coefficients with edge ratio and taper amount, for linear and exponential thickness variation, and for various boundary conditions. Using the classical theory of plates and the numerical solution of the governing differential equation, Gupta et al. [8] investigated the buckling and vibrations of polar orthotropic annular plates of variable thickness. Harik et al. [9] developed the elastic stability of plates which have different stiffness and under in-plane loads. Here, the authors used the classical method of separation of variables and the classical finite difference technique to solve the higher order differential equations. Nerantzaki et al. [10] discussed the stability of plates that has variable thickness along the x-axis using the analog equation method.

It is clear that the elastic base causes the plate to become stiffer. Therefore, when the plates are located on different elastic bases, it is necessary to carefully consider the influence of the foundation on the stability of the plates. The mechanical buckling and free vibration of thick plates resting on Pasternak elastic foundation subjected to in-plane loading is studied by Hamid et al. [11] using the third order shear deformation theory and the spline finite strip method. Shen [12] investigated the thermoelastic buckling and postbuckling of plates lying on elastic base when plates were placed under temperature changes, thermally induced compressive stresses are increased in the constraint plate.

Actually, there has not been few research on stability analysis of cracked plates with nonlinearly varying thickness resting on the elastic foundations according to Shi's HSDT [13] and Phase-Field theory. Therefore, this study will focus on investigating the influence of plate edge ratio, crack length, crack inclination angle, crack location, plate thickness ratio and the influence of elastic foundations on stability of plate.

2 The HSDT of plate with nonlinearly variable thickness and phase-field theory

This research introduces a finite element formula for the plate using Shi's the third-order shear deformation theory [13] based on the strict kinematic assumption of displacement. It can be seen that the kinematics of the displacement which is derived from the elastic formula is closer to the finite element method than from the displacement hypothesis. The displacements (U_x, U_y, U_z) at any point (x, y, z) in the plate can be represented as five unknown variables as expression (1):

$$\begin{aligned}
U_x(x,y,z) &= U_{0x}(x,y) + \frac{5}{4}\left(z - \frac{4}{3h^2(x)}z^3\right)\theta_x(x,y) + \left(\frac{1}{4}z - \frac{5}{3h^2(x)}z^3\right)\frac{\partial U_{0z}(x,y)}{\partial x} \\
U_y(x,y,z) &= U_{0y}(x,y) + \frac{5}{4}\left(z - \frac{4}{3h^2(x)}z^3\right)\theta_y(x,y) + \left(\frac{1}{4}z - \frac{5}{3h^2(x)}z^3\right)\frac{\partial U_{0z}(x,y)}{\partial y} \\
U_z(x,y,z) &= U_{0z}(x,y)
\end{aligned} \tag{1}$$

$$\begin{Bmatrix} \boldsymbol{\varepsilon}_x \\ \boldsymbol{\varepsilon}_y \\ \boldsymbol{\varepsilon}_{xy} \\ \boldsymbol{\gamma}_{yz} \\ \boldsymbol{\gamma}_{xz} \end{Bmatrix} = \begin{Bmatrix} U_{0x,x} + z\frac{1}{4}(5\theta_{x,x} + U_{z,xx}) + z^3\left(\frac{-5}{3h^2}\right)\left[\theta_{x,x} + U_{z,xx} + \left(\frac{-2}{h}\right)h_{,x}\left(\theta_x + U_{z,x}\right)\right] \\ U_{0y,y} + z\frac{1}{4}(5\theta_{y,y} + U_{z,yy}) + z^3\left(\frac{-5}{3h^2}\right)(\theta_{y,y} + U_{z,yy}) \\ U_{0x,y} + U_{0y,x} + z\frac{1}{4}(5\theta_{x,y} + 2U_{z,xy} + 5\theta_{y,x}) + \\ \qquad + z^3\left(\frac{-5}{3h^2}\right)\left[\theta_{x,y} + 2U_{z,xy} + \theta_{y,x} + \left(\frac{-2}{h}\right)h_{,x}\left(\theta_y + U_{z,y}\right)\right] \\ \frac{5}{4}(\theta_y + U_{z,y}) + z^2\left(\frac{-5}{h^2}\right)(\theta_y + U_{z,y}) \\ \frac{5}{4}(\theta_x + U_{z,x}) + z^2\left(\frac{-5}{h^2}\right)(\theta_x + U_{z,x}) \end{Bmatrix} \tag{2}$$

Where U_x, U_y, U_z respectively are the displacements at the middle plane of the plate in the x, y, z axes; θ_x, θ_y are the normal rotation angles of the mid-plate along the x, y axes. The commas describe the derivatives corresponding to the variables x, y.

According to Hooke's law, the relationship of strain and stress components is introduced through the following equations:

$$\begin{cases} \boldsymbol{\sigma} = \boldsymbol{D}_m(\boldsymbol{\varepsilon}_0 + z\boldsymbol{\varepsilon}_1 + z^3\boldsymbol{\varepsilon}_3) \\ \boldsymbol{\tau} = \boldsymbol{D}_s(\boldsymbol{\gamma}_0 + z^2\boldsymbol{\gamma}_2) \end{cases} \tag{3}$$

with $\boldsymbol{\sigma} = \begin{bmatrix} \sigma_x & \sigma_y & \sigma_{xy} \end{bmatrix}^T$; $\boldsymbol{\tau} = \begin{bmatrix} \tau_{yz} & \tau_{xz} \end{bmatrix}^T$

$$\boldsymbol{D}_m = \frac{E}{1-\upsilon^2}\begin{bmatrix} 1 & \upsilon & 0 \\ \upsilon & 1 & 0 \\ 0 & 0 & \frac{1}{2}(1-\upsilon) \end{bmatrix}; \quad \boldsymbol{D}_s = \frac{E}{2(1+\upsilon)}\begin{bmatrix} 1 & 0 \\ 0 & 1 \end{bmatrix} \tag{4}$$

where E is Young's modulus; υ is the Poisson's ratio. And note that the symbol $\boldsymbol{\varepsilon}_0$; $\boldsymbol{\varepsilon}_1$; $\boldsymbol{\varepsilon}_3$; $\boldsymbol{\gamma}_0$; $\boldsymbol{\gamma}_2$ in equation (3) is the strain components in equation (2) of the displacements in the plate [13].

The components of normal force, bending moment, higher-order moment and shear force according to the HSDT of Shi [13] are introduced according to the equations:

$$\begin{Bmatrix} \bar{\boldsymbol{N}} \\ \bar{\boldsymbol{M}} \\ \bar{\boldsymbol{P}} \\ \bar{\boldsymbol{Q}} \\ \bar{\boldsymbol{R}} \end{Bmatrix} = \begin{bmatrix} \bar{\boldsymbol{A}} & \bar{\boldsymbol{B}} & \bar{\boldsymbol{E}} & 0 & 0 \\ \bar{\boldsymbol{B}} & \bar{\boldsymbol{D}} & \bar{\boldsymbol{F}} & 0 & 0 \\ \bar{\boldsymbol{E}} & \bar{\boldsymbol{F}} & \bar{\boldsymbol{H}} & 0 & 0 \\ 0 & 0 & 0 & \boldsymbol{A} & \boldsymbol{B} \\ 0 & 0 & 0 & \boldsymbol{B} & \boldsymbol{D} \end{bmatrix} \begin{Bmatrix} \boldsymbol{\varepsilon}_0 \\ \boldsymbol{\varepsilon}_1 \\ \boldsymbol{\varepsilon}_3 \\ \boldsymbol{\gamma}_0 \\ \boldsymbol{\gamma}_2 \end{Bmatrix} \tag{5}$$

where

$$(\bar{\boldsymbol{H}}, \bar{\boldsymbol{F}}, \bar{\boldsymbol{E}}, \bar{\boldsymbol{D}}, \bar{\boldsymbol{B}}, \bar{\boldsymbol{A}}) = \int_{-h/2}^{h/2} (z^6, z^4, z^3, z^2, z, 1)\boldsymbol{D}_m dz; \ (\boldsymbol{D}, \boldsymbol{B}, \boldsymbol{A}) = \int_{-h/2}^{h/2} (z^4, z^2, 1)\boldsymbol{D}_s dz \tag{6}$$

On the basis of elastic theory, the strain energy of the plate (Π) can be written as:

$$\Pi(\boldsymbol{q}) = \frac{1}{2}\int_\Omega \begin{pmatrix} \boldsymbol{\varepsilon}_0^T \bar{\boldsymbol{A}}\boldsymbol{\varepsilon}_0^T + \boldsymbol{\varepsilon}_0^T \bar{\boldsymbol{B}}\boldsymbol{\varepsilon}_1 + \boldsymbol{\varepsilon}_0^T \bar{\boldsymbol{E}}\boldsymbol{\varepsilon}_3 + \\ + \boldsymbol{\varepsilon}_1^T \bar{\boldsymbol{B}}\boldsymbol{\varepsilon}_0 + \boldsymbol{\varepsilon}_1^T \bar{\boldsymbol{D}}\boldsymbol{\varepsilon}_1 + \boldsymbol{\varepsilon}_1^T \bar{\boldsymbol{F}}\boldsymbol{\varepsilon}_3 + \\ + \boldsymbol{\varepsilon}_3^T \bar{\boldsymbol{E}}\boldsymbol{\varepsilon}_0 + \boldsymbol{\varepsilon}_3^T \bar{\boldsymbol{F}}\boldsymbol{\varepsilon}_1 + \boldsymbol{\varepsilon}_3^T \bar{\boldsymbol{H}}\boldsymbol{\varepsilon}_3 + \\ + \boldsymbol{\gamma}_0^T \boldsymbol{A}\boldsymbol{\gamma}_0 + \boldsymbol{\gamma}_0^T \boldsymbol{B}\boldsymbol{\gamma}_2 + \boldsymbol{\gamma}_2^T \boldsymbol{B}\boldsymbol{\gamma}_0 + \boldsymbol{\gamma}_2^T \boldsymbol{D}\boldsymbol{\gamma}_2 \end{pmatrix} d\Omega \tag{7}$$

where $\Pi(\boldsymbol{q})$ is the potential energy of the plate in the absence of cracks; $\boldsymbol{q}$ is displacement vector.

The energy of the elastic foundation Pasternak acting on the plate:

$$\Pi^e(\boldsymbol{q}, s) = \frac{1}{2}\int_\Omega s^2 \left\{ k_w U_z^2 + k_s \left[\left(\frac{\partial U_z}{\partial x} \right)^2 + \left(\frac{\partial U_z}{\partial y} \right)^2 \right] \right\} d\Omega \tag{8}$$

with k_w, k_s are the coefficients of the elastic foundation Pasternak. In the case of the plate supported on a Winkler foundation, k_s is zero.

To simulate the state of a material, phase field theory introduces a scalar variable *s*. When the material is in the crack region, the variable *s* is between 0 and 1. For the material in the fully cracked state, *s*=0. In contrast, for a material in its normal state, *s*=1. In the strain energy expression, the variable *s* is added to show that when the plate is cracked, the energy is reduced.

The total strain energy for the plate can be determined by equation (9):

$$\begin{aligned}\Pi^t(\boldsymbol{q},s) &= \Pi(\boldsymbol{q},s)+\Pi^e(\boldsymbol{q},s)\\ &= \left\{\begin{array}{l}\dfrac{1}{2}\int_\Omega s^2\left(\begin{array}{l}\boldsymbol{\varepsilon}_0^T\bar{\boldsymbol{A}}\boldsymbol{\varepsilon}_0^T+\boldsymbol{\varepsilon}_0^T\bar{\boldsymbol{B}}\boldsymbol{\varepsilon}_1+\boldsymbol{\varepsilon}_0^T\bar{\boldsymbol{E}}\boldsymbol{\varepsilon}_3+\\ +\boldsymbol{\varepsilon}_1^T\bar{\boldsymbol{B}}\boldsymbol{\varepsilon}_0+\boldsymbol{\varepsilon}_1^T\bar{\boldsymbol{D}}\boldsymbol{\varepsilon}_1+\boldsymbol{\varepsilon}_1^T\bar{\boldsymbol{F}}\boldsymbol{\varepsilon}_3+\\ +\boldsymbol{\varepsilon}_3^T\bar{\boldsymbol{E}}\boldsymbol{\varepsilon}_0+\boldsymbol{\varepsilon}_3^T\bar{\boldsymbol{F}}\boldsymbol{\varepsilon}_1+\boldsymbol{\varepsilon}_3^T\bar{\boldsymbol{H}}\boldsymbol{\varepsilon}_3+\\ +\boldsymbol{\gamma}_0^T\boldsymbol{A}\boldsymbol{\gamma}_0+\boldsymbol{\gamma}_0^T\boldsymbol{B}\boldsymbol{\gamma}_2+\boldsymbol{\gamma}_2^T\boldsymbol{B}\boldsymbol{\gamma}_0+\boldsymbol{\gamma}_2^T\boldsymbol{D}\boldsymbol{\gamma}_2\end{array}\right)d\Omega+\\ +\dfrac{1}{2}\int_\Omega s^2\left\{k_wU_z^2+k_s\left[\left(\dfrac{\partial U_z}{\partial x}\right)^2+\left(\dfrac{\partial U_z}{\partial y}\right)^2\right]\right\}d\Omega+\\ +\dfrac{1}{2}\int_\Omega s^2\begin{bmatrix}U_{z,x} & U_{z,y}\end{bmatrix}\tilde{\sigma}^0\begin{bmatrix}U_{z,x} & U_{z,y}\end{bmatrix}^T h d\Omega+\\ +\dfrac{1}{2}\int_\Omega s^2\begin{bmatrix}\theta_{x,x} & \theta_{x,y}\end{bmatrix}\tilde{\sigma}^0\begin{bmatrix}\theta_{x,x} & \theta_{x,y}\end{bmatrix}^T\dfrac{h^3}{12}d\Omega+\\ +\dfrac{1}{2}\int_\Omega s^2\begin{bmatrix}\theta_{y,x} & \theta_{y,y}\end{bmatrix}\tilde{\sigma}^0\begin{bmatrix}\theta_{y,x} & \theta_{y,y}\end{bmatrix}^T\dfrac{h^3}{12}d\Omega+\\ +\int_\Omega G_C h\left[\dfrac{(1-s)^2}{4l_c}+l_c|\nabla s|^2\right]d\Omega\end{array}\right.\\ &= \left\{\int_\Omega s^2\Gamma(\boldsymbol{q})d\Omega+\int_\Omega G_C h\left[\dfrac{(1-s)^2}{4l_c}+l_c|\nabla s|^2\right]d\Omega\right\}\end{aligned} \tag{9}$$

where G_C is surface energy in Griffith's theory and l_c is a positive constant used to represent the crack width.

$$\bar{\sigma}^0=\begin{bmatrix}\bar{\sigma}_x^0 & \bar{\tau}_{xy}^0\\ \bar{\tau}_{xy}^0 & \bar{\sigma}_y^0\end{bmatrix} \tag{10}$$

with $\bar{\sigma}_x^0$, $\bar{\sigma}_y^0$ respectively are the normal stresses of the plate for the x, y axes,; $\bar{\tau}_{xy}^0$ is the shear stress of the plate in the x-y plane, at the time of external forces acting on the plate edges.

The first-order variation of function $\Pi^t(\boldsymbol{q},s)$ with respect to variables $\boldsymbol{q},s$ is defined by formula (11) as follows:

$$\begin{cases}\delta\Pi^t(\boldsymbol{q},s,\delta\boldsymbol{q})=0\\ \delta\Pi^t(\boldsymbol{q},s,\delta s)=0\end{cases} \tag{11}$$

From equation (11), the equations for calculating the instability of the cracked plate are shown as follows:

$$\left(\sum\mathbf{K}^e+\lambda_{cr}\sum\mathbf{K}_G^e\right)\boldsymbol{q}=0 \tag{12}$$

$$\int_\Omega 2s\Gamma(\boldsymbol{q})\delta s d\Omega+\int_\Omega 2G_C h\left[-\frac{(1-s)}{4l_c}+l_c\nabla s\nabla(\delta s)\right]d\Omega=0 \tag{13}$$

Substituting the value of *s* calculated from equation (13) into equation (12), we can find the critical buckling load λ_{cr}. In Equation (13), the shape of the crack is described by the function $\Gamma(\boldsymbol{q})$ according to Michael et al. [15] as follows:

$$\Gamma(\boldsymbol{q}) = B_0 \frac{G_C}{4l_c}.\mathrm{L}_0(x,y) \tag{14}$$

where $L_0(x,y) = \begin{cases} \left(1-\dfrac{d(x,y)}{l_c}\right) & if \ \dfrac{-c.\sin\beta}{2} \le x-\dfrac{a}{2} \le \dfrac{c.\sin\beta}{2} \ and \ \dfrac{-l_c}{2} \le y-\dfrac{b}{2}+\left(x-\dfrac{a}{2}\right)\cot\beta \le \dfrac{l_c}{2} \\ 0 & else \end{cases}$

where scalar magnitude B_0 is taken as $B = 10^3$; β and c are the crack inclination angle and length (Fig. 3), respectively; l_c is the width of the crack; $d(x,y)$ is the minimum distance from any point (x,y) to the crack boundary; a and b are the dimensions of the two sides of the plate.

3 Numerical results

3.1 The instability coefficient of the non-cracked plate with the thickness varies exponentially.

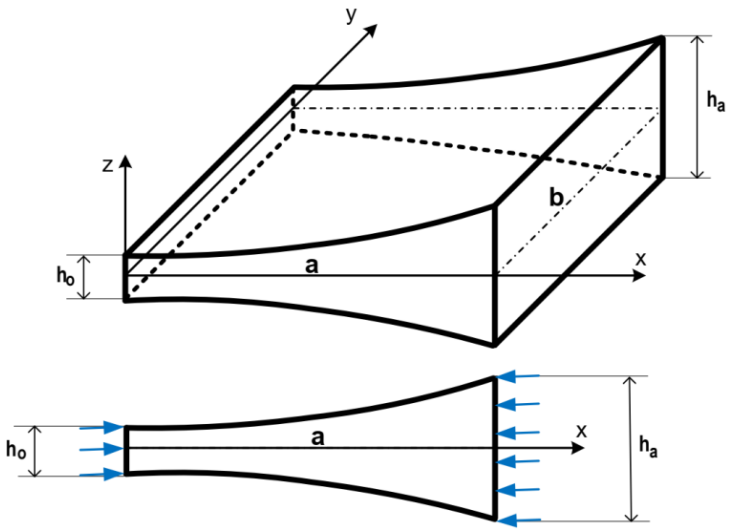

Fig. 1 - The uncracked plate with exponential thickness variation under uniaxial compression force in x-direction

The buckling factor of the non-cracked plate which has exponential varying thickness has been compared with the results from references [9, 10]. The thickness of the plate varies with the formula $h = h_0 e^{\frac{x}{a}\ln\frac{h_a}{h_0}}$. The length-width ratio of the plate examined: $\frac{a}{b} = 0.5;\ 1.0;\ 1.5;\ 2.0$, the plate thickness ratio is also calculated according to the data: $\frac{h_a}{h_o} = 1.125;\ 1.25;\ 1.5;\ 1.75;\ 2.0$. During the calculation, Young's modulus is taken: $E = 70GPa$, Poisson ratio $\upsilon = 1/3$. The plate is compressed along the x-axis (as shown in Fig. 1) and the boundary condition at the four sides is simple support (SSSS).The instability coefficient is calculated as a dimensionless value according to the following formula [10]:

$$\lambda_M = \frac{\lambda_{cr} b^2}{\pi^2 D_M} \tag{15}$$

where $D_M = \dfrac{Eh_M^3}{12(1-\upsilon^2)}$; $h_M = \sqrt{h_0 h_a}$

Table 1 - The non-dimensionalized instability coefficient λ_M of plate subjected to uniaxial compression load in the x direction. Upper row: Harik et al. [9], Middle row: M.S. Nerantzaki [10], Lower row: This study.

	h_a/h_0				
a/b	1.125	1.25	1.5	1.75	2
0.5	6.45	7.339	6.67	6.995	7.455
	6.28	6.224	6.05	5.838	5.615
	6.2215	6.1742	6.0295	5.8419	5.6543
1	4.073	4	3.95	3.843	3.686
	4	3.922	3.698	3.451	3.212
	3.9686	3.8976	3.6943	3.469	3.2547
1.5	4.184	3.949	3.541	3.206	2.933
	4.21	3.924	3.417	3.008	2.678
	4.1477	3.8784	3.4015	3.0187	2.7091
2	3.897	3.674	3.224	2.85	2.552
	3.925	3.644	3.141	2.712	2.37
	3.869	3.6116	3.1175	2.7157	2.3972

The buckling coefficients of plate with an exponential change in thickness for each plate size is shown in Table 1. It is easy to see that the calculated results of this study are close to the results that Harik et al. [9] and Nerantzaki [10] studied. This shows that the calculation program of this study is quite accurate. On that basis, we develop a calculation program for variable thickness plates with cracks.

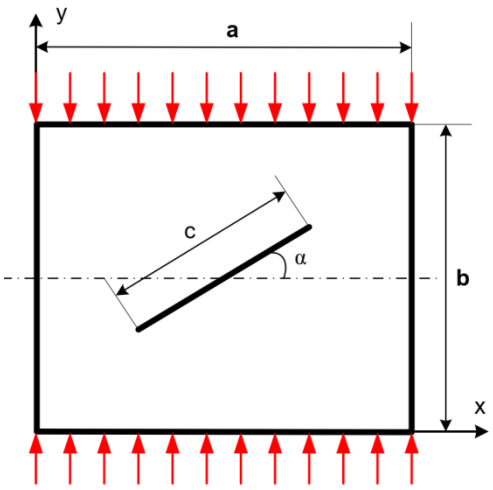

Fig. 2 - The square cracked plate subjected to compression loadin the y-axis direction

3.2 Critical buckling load of cracked rectangular plate with constant thickness

In this part, another example in investigating the critical buckling load of cracked plates using phase field theory will be presented. The selected plate has the constant thickness: $h = 1.2\,mm$, a crack of length c, an angle of inclination α as shown in ***Fig. 2***. The dimensions of the square plate with equal length and width up to 0.24 *m*, are taken as in the reference of Rahman et al. [14]. Here, the plate boundary condition is set to clamp two opposite faces in the y-axis direction, the other two faces are free. Calculation results with the following data: the crack is located in the center of plate with the ratio of the crack length to the plate length (c/a) taking values of 0.3 and 0.5; and crack inclination angle (α) is changed with 3 cases: 0 degrees, 30 degrees, 60 degrees. The critical buckling load of plate is determined by formula (16) as follows:

$$N_{cr} = \frac{\lambda_{cr}\pi^2 D_c}{b^2} \tag{16}$$

where $D_c = \frac{Eh^3}{12(1-\upsilon^2)}$

Table 2 – The critical buckling load of the cracked square plate

c/a	*α°*	Rahman et al. [14]		Present	% Err Experiment
		FEM	Experiment		
0	-	1792.2	1718	1813.02	5.24%
0.3	0	1602.48	1531	1538.12	0.46%
0.5		1351.3	1317	1206.52	-9.16%
0.3	30	1669.68	1551	1629.67	4.83%
0.5		1516.10	1396	1413.85	1.26%
0.3	60	1753.49	1660	1755.81	5.46%
0.5		1701.34	1636	1723.98	5.10%

The results of the present method have been compared to the results of Rahman et al. [14] (Table 2). The calculated critical buckling loads are very close to the results in the reference paper. In reference [15], the authors investigated the critical load on the basis of the finite element method (FEM) and experiment. In this study, the HSDT for plate combined with phase-field theory and the finite element method (FEM) is used to calculate the critical load. The calculated value shown in Table 2 is actually close to the FEM result of the comparison document. The fact that the error is not small compared to the experiment is acceptable because the experimental sample has an error in size when processing and creating the sample.

3.3 The buckling coefficients of the cracked plate with nonlinearly variable thickness resting on elastic foundations.

In this part, the buckling coefficients of rectangular cracked plates with the length (*a*), the width *b* = 0.24*m* and exponential variation in thickness along the x-axis (plate length) are calculated. The plate thickness varies exponentially according to the formula $h = h_0 e^{\frac{x}{a}\ln\frac{h_a}{h_0}}$ [10], where h_0 is minimum thickness of the plate on the edge along the y-axis with $h_0 = b/100$, the plate thickness h_a varies depending on h_0. Poisson's ratio and Young's modulus are the same as in section 3.1: $\upsilon = 1/3$ and $E = 70GPa$. The cracked plate is placed on the two-parameter elastic foundation (Pasternak foundation) as illustrated in Fig. 3. The stability factor is studied based on the change of the length and location of the crack, the crack length (*c*) will be affected as 50%, 30%, 10% and 0 (no cracks) of the plate length (*a*), the crack is located in the center of the plate with the inclined angles investigated in the different cases 0 degrees, 30 degrees and 60 degrees. The boundary conditions of the plates is full simple support (SSSS) when subjected to uniaxial compressive loads on opposite sides in the x-axis. The buckling coefficient is calculated according to the following formula (15).

Here, the corresponding unitless elastic foundation coefficients according to the formula (17):

$$\bar{k}_w = \frac{k_w a^4}{D_M};\ \ \bar{k}_s = \frac{k_s a^2}{D_M} \tag{17}$$

with $D_M = \frac{Eh_M^3}{12(1-\upsilon^2)};\ \ h_M = \sqrt{h_0 h_a}$

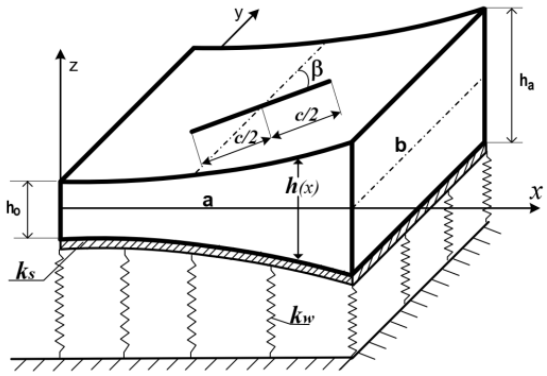

Fig. 3 - The cracked rectangular plate with nonlinearly variable thickness under the compression load in x-axis direction

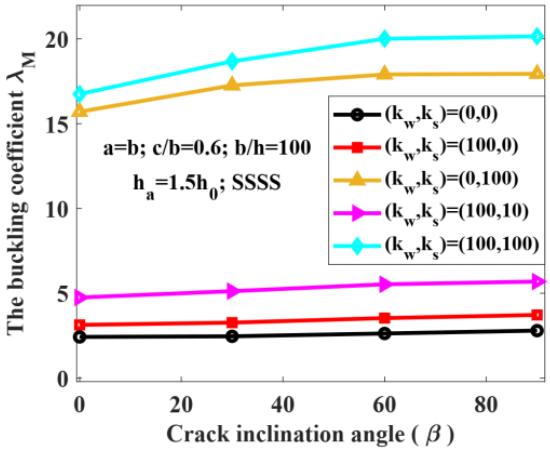

Fig. 4 – The stability coefficient of the cracked plate with the change of the elastic foundation and the crack inclination angle.

The numerical results are described in Table 3, Table 4 and Fig. 4, Fig. 5 as follows.

Table 3 – The buckling coefficient (λ_M) of the cracked square plate with $(\bar{k}_w, \bar{k}_s) = (50, 0)$

c/b	β^0	h_a/h_0				
		1.125	1.25	1.5	1.75	2
0	-	4.48241	4.39071	4.13766	3.86839	3.61639
0.1	0	4.39167	4.31599	4.09651	3.84959	3.60976
0.3		3.83864	3.82393	3.76882	3.67251	3.53359
0.5		3.05771	3.06606	3.09485	3.13116	3.16584
0.1	30	4.3961	4.31859	4.09559	3.84688	3.60667
0.3		3.88727	3.86312	3.78046	3.65809	3.50588
0.5		3.15966	3.16211	3.16991	3.17339	3.1626
0.1	60	4.39506	4.31565	4.08915	3.83903	3.59901
0.3		3.95926	3.91806	3.78969	3.62807	3.45438
0.5		3.40132	3.38149	3.31855	3.23427	3.13605
0.1	90	4.39517	4.31475	4.08627	3.83513	3.59487
0.3		4.00025	3.95076	3.80114	3.62154	3.43653
0.5		3.55962	3.52627	3.42433	3.2985	3.1645

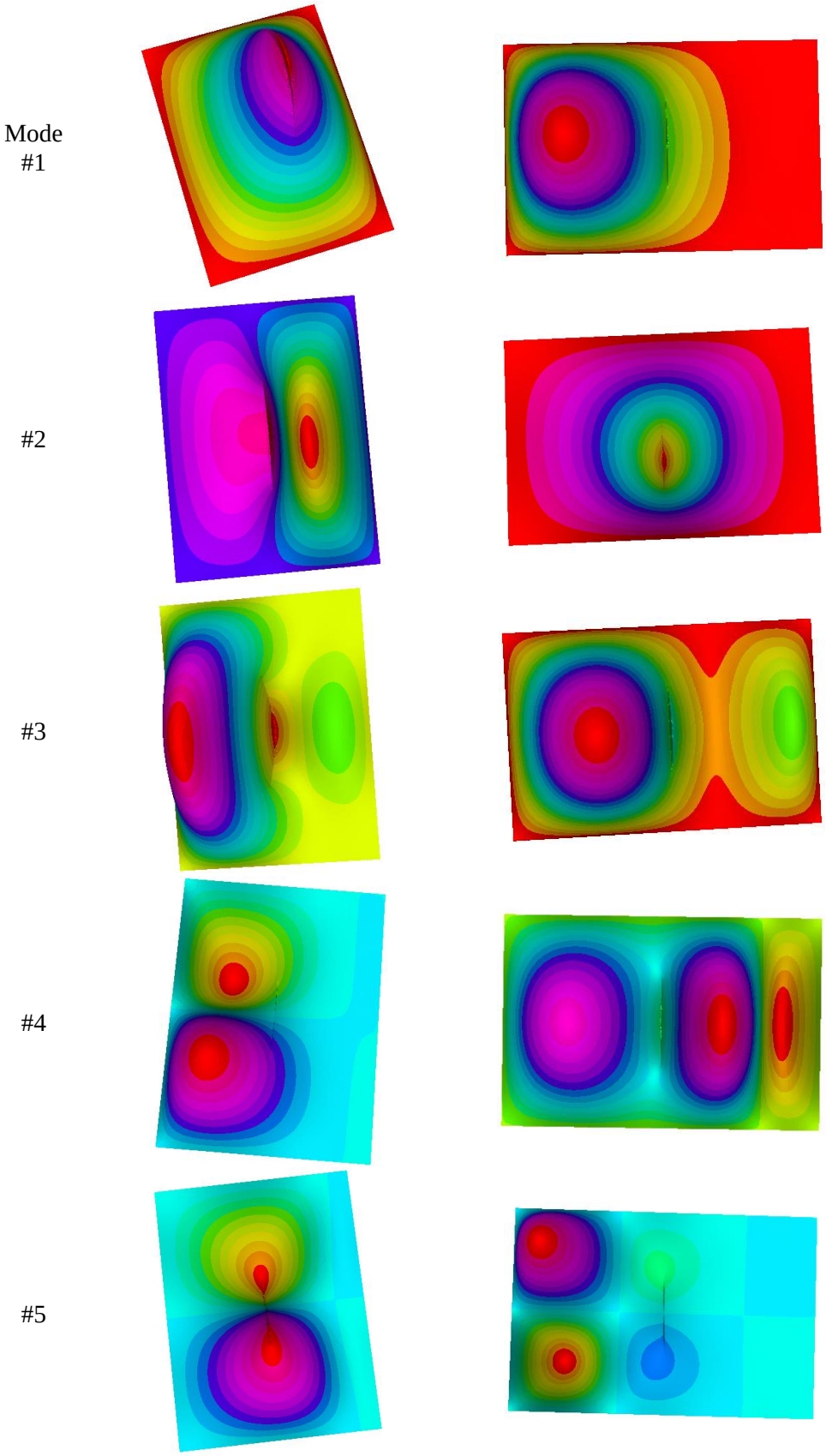

a. Cracked plate with a=0.75b b. Cracked plate with a=1.5b

Fig. 5 – The first five mode of instability of cracked plate with $h_a = 1.5h_0$; $c = 0.4b$; $\beta = 0^0$; $(\bar{k}_w, \bar{k}_s) = (0,0)$

Table 3 shows that the crack length has a significant influence on the plate stability. When the plate has a crack, it reduces the stiffness of the plate, the larger the crack, the lower the hardness of the plate, leading to a corresponding decrease in the buckling coefficient. This is very evident when the crack length reaches 50% of the plate width (c/b = 0.5), then the stability coefficient is the smallest compared to the case of smaller cracks or no cracks. It is clear that, with the increased plate thickness ratio (h_a/h_0), there is greater stress in the thin part of the plate, leading to more rapid plate instability.

Fig. 4 shows that, when the crack angle increases, the crack rotates towards parallel to the x-axis (the axis has the compressive forces on the plate), the crack surface under the influence of the compressive force gradually decreases, causing a small decrease in the stiffness of the plate. Thus, the stability coefficient is the largest when the crack inclination angle is 90^0. This is also shown in Table 3 and Table 4.

Table 4 – The buckling coefficient (λ_M) **of the cracked square plate with** $h_a = 1.5h_0;\ c = 0.4b;\ (\bar{k}_w, \bar{k}_s) = (0,0)$

	a/b						
β^0	0.5	0.75	1	1.25	1.5	1.75	2
0	3.16558	2.90033	3.01135	3.28083	3.41682	3.14465	2.97496
30	3.65901	3.04518	3.04078	3.25992	3.40578	3.2193	3.03712
60	4.80558	3.36479	3.09988	3.18061	3.30332	3.24836	3.11097
90	5.36279	3.5456	3.14827	3.15498	3.24492	3.229	3.12813

With the quantities $h_a = 1.5h_0;\ c = 0.4b;\ (\bar{k}_w, \bar{k}_s) = (0,0)$ being constant and paying attention to the compressive force along the x-axis, the plate edge ratio a/b has a great influence on the plate's stability coefficient (Table 4).

Figure 5 depicts the first five types of instability of a plate with a central crack as the thickness varies nonlinearly along the length of the plate. Here, we can see that for a=0.75b the first mode of instability occurs at the crack location, while for a=1.5b it occurs in half of the plate where the thickness is small.

4 Conclusions

This study investigates the stability of cracked plate with nonlinearly varying thickness resting on Pasternak elastic foundation according to HSDT and phase field theory. Numerical results show that: (i) as the crack length increases, the crack area of the plate is reduced in elastic energy, resulting in a decrease in the buckling coefficient of the plates; (ii)when the crack angle increases, the stability coefficients of the plate will change depending on the aspect ratio of the plate; (iii) when the plate thickness ratio h_a/h_0 increases (h_0 = constant), the plate becomes more slender leading to faster instability; (iv) when the Pasternak coefficient increases, the foundation hardness increases, making the plate have a higher hardness, so the stability coefficient of the plate increases. This numerical result will serve as a guide for studies on the stability of the plate resting on elastic foundations as the crack develops.

Acknowledgements

This research is funded by Vietnam Ministry of Education and Training under grant number B2022-GHA-02.

REFERENCES

[1]- Minh, P.P. and N.D. Duc, The effect of cracks on the stability of the functionally graded plates with variable-thickness using HSDT and phase-field theory. Composites Part B, 175 (2019) 107086. doi:10.1016/j.compositesb.2019.107086.

[2]- Minh, P.P. and N.D. Duc, The effect of cracks and thermal environment on free vibration of FGM plates. Thin-Walled Structures, 159 (2021) 107291. doi:10.1016/j.tws.2020.107291.

[3]- Minh, P.P., D.T. Manh, and N.D. Duc, Free vibration of cracked FGM plates with variable thickness resting on elastic foundations. Thin-Walled Structures, 161 (2021) 107425. doi:10.1016/j.tws.2020.107425.

[4]- Duc, N.D. and P.P. Minh, Free vibration analysis of cracked FG CNTRC plates using phase field theory. Aerospace

Science and Technology, 112 (2021) 106654. doi:10.1016/j.ast.2021.106654.

[5]- Phuc, P.M., Anynasys free vibration of the functionally grade material cracked plates with varying thickness using the phase-field theory. Transp. Commun. Sci. J., 70(2) (2019) 122-131. doi:10.25073/tcsj.70.2.35.

[6]- Minh, P.P., Using phase field and third-order shear deformation theory to study the effect of cracks on free vibration of rectangular plates with varying thickness. Transp. Commun. Sci. J., 71(7) (2020) 853-867. doi:10.47869/tcsj.71.7.10.

[7]- Wittrick, W.H. and C.H. Ellen, Buckling of Tapered Rectangular Plates in Compression. Aeronautical Quarterly, 13(4) (2016) 308-326. doi:10.1017/S0001925900002547.

[8]- Gupta, U.S., R. Lal, and C.P. Verma, Buckling and vibrations of polar orthotropic annular plates of variable thickness. J. Sound Vibrat., 104(3) (1986) 357-369. doi:10.1016/0022-460X(86)90294-4.

[9]- Harik, I.E., X. Liu, and R. Ekambaram, Elastic stability of plates with varying rigidities. Comput. Str., 38(2) (1991) 161-169. doi:10.1016/0045-7949(91)90094-3.

[10]- Nerantzaki, M.S. and J.T. Katsikadelis, Buckling of plates with variable thickness—an analog equation solution. Engineering Analysis with Boundary Elements, 18(2) (1996) 149-154. doi:10.1016/S0955-7997(96)00045-8.

[11]- Foroughi, H. and M. Azhari, Mechanical buckling and free vibration of thick functionally graded plates resting on elastic foundation using the higher order B-spline finite strip method. Meccanica, 49(4) (2014) 981-993. doi:10.1007/s11012-013-9844-2.

[12]- Shen, H.-S., Thermoelastic Buckling and Postbuckling of Plates on Elastic Foundations, in Encyclopedia of Thermal Stresses, R.B. Hetnarski, Editor. Springer Netherlands: Dordrecht. (2014), 5644-5653. doi:10.1007/978-94-007-2739-7_518.

[13]- Shi, G., A new simple third-order shear deformation theory of plates. Int. J. Sol. Str., 44(13) (2007) 4399-4417. doi:10.1016/j.ijsolstr.2006.11.031.

[14]- Seifi, R. and N. Khoda-yari, Experimental and numerical studies on buckling of cracked thin-plates under full and partial compression edge loading. Thin-Walled Structures, 49(12) (2011) 1504-1516. doi:10.1016/j.tws.2011.07.010.

[15]- Borden, M.J., C.V. Verhoosel, M.A. Scott, T.J.R. Hughes, and C.M. Landis, A phase-field description of dynamic brittle fracture. Comput. Methods Appl. Mech. Eng., 217-220 (2012) 77-95. doi:10.1016/j.cma.2012.01.008.